Talanta 105 (2013) 229–234

Contents lists available at SciVerse ScienceDirect

Talanta

journal homepage: www.elsevier.com/locate/talanta

Electrochemical synthesis of Fe_2O_3 on graphene matrix for indicator-free impedimetric aptasensing

Meng Du [1], Tao Yang [1], Xiuhong Guo, Ling Zhong, Kui Jiao *

College of Chemistry and Molecular Engineering, Qingdao University of Science and Technology, Qingdao 266042, China.

ARTICLE INFO

Article history:
Received 22 August 2012
Received in revised form
17 November 2012
Accepted 24 November 2012
Available online 1 December 2012

Keywords:
Graphene
Fe_2O_3
Electrodeposition
Indicator-free impedance
Lysozyme

ABSTRACT

Herein, an electrochemical platform was employed for the detection of protein. Fe_2O_3 was electrochemically deposited on graphene modified glassy carbon electrode surface. Electrodeposition conditions, such as temperature, and time, were optimized for controlling morphologies and electrochemical activities of Fe_2O_3. Negatively charged lysozyme-binding aptamer (LBA) was immobilized on positively charged Fe_2O_3 (isoelectric point ~7.0) via electrostatic interaction. Electrochemical impedance spectroscopy was adopted for indicator-free detection of lysozyme. The LBA on the outermost layer would catch lysozyme in solution by physical affinity, which induced the increase of impedimetric signals. In this strategy, a wide detection range (0.5 ng mL^{-1}–5 μg mL^{-1}) and low detection limit (0.16 ng mL^{-1}) for model target lysozyme was obtained. The results showed that indicator-free impedimetric aptasensing strategy had good sensitivity and selectivity.

1. Introduction

Graphene attracts tremendous attention since its discovery by Novoselov and Geim in 2004 [1]. The attributes, such as large surface area, excellent conductivity and high transparency, make graphene a novel substrate for forming hybrid structures with a variety of nanomaterials [2]. Graphene-based nanocomposites can exhibit excellent properties of parent constituents in appropriate designs [3]. Much effort has been devoted to incorporate graphene and metal oxides into composite materials including graphene–ZrO_2 [4], graphene–SnO_2 [5], graphene–TiO_2 [6], graphene–ZnO [7], graphene–Co_3O_4 [8], graphene–RuO_2 [9], and graphene–Fe_3O_4 [10]. These graphene–metal oxide composites are widely employed in theory and applications like electronics, optics, electrochemical energy conversion and storage, and solar energy harvesting. To the best of our knowledge, electrochemical aptasensor based on graphene–metal oxide composite materials has not been reported.

Among numerous metal oxides, Fe_2O_3 may act as a promising substrate for biosensing [11,12]. However, Fe_2O_3 suffers from poor electrochemical performance due to the agglomerations and huge volume change. Various attempts have been reported to overcome the disadvantages of Fe_2O_3 [13,14]. The synthesis of Fe_2O_3 with special sizes and well-defined morphologies has become a hot topic in material research field [15]. Compared with chemical synthesis, electrochemical deposition technique is a low-temperature, low-cost, and facile method for the synthesis of graphene–metal oxide composites [16,17]. Electrochemical deposition of Fe_2O_3 on graphene support needs to be explored.

In recent years, electrochemical impedance spectroscopy (EIS) is rapidly developing in label-free biosensors, which is useful for bioanalysis to bypass the modification of biomolecules with complex labels [18]. However, EIS is hard to meet the requirement for on-line monitoring due to the adoption of external redox indicator [19]. Indicator-free EIS has been reported for protein adsorption study [20] and DNA sensing [21].

In this work, an innovative aptasensor was developed on electrochemically converted Fe_2O_3/graphene substrate. In detail, graphene oxide (GNO) was firstly coated on glassy carbon electrode surface to form a stable film. Then GNO was electrochemically reduced to graphene. Fe_2O_3 was electrodeposited on graphene substrate using constant potential technique. The effect of deposition temperature and deposition time on the morphology of Fe_2O_3 was studied by scanning electron microscopy (SEM) and electrochemistry. The prepared Fe_2O_3/graphene nanocomposites exhibited high conductivity and large electroactive area. Lysozyme-binding aptamer (LBA) could be immobilized on Fe_2O_3/graphene nanocomposites by electrostatic interaction. LBA on the outmost layer of biosensor could bind target protein lysozyme in solution to form lysozyme–aptamer complex because of the high affinity of lysozyme and LBA. The binding would increase the interfacial electron transfer resistance. This aptasensor could be used for indicator-free electrochemical detection of lysozyme with EIS.

* Corresponding author. Tel.: +86 532 84022665; fax: +86 532 84023927.
E-mail address: kjiao@qust.edu.cn (K. Jiao).
[1] These authors contributed equally to this work.

0039-9140/$ - see front matter © 2012 Elsevier B.V. All rights reserved.
http://dx.doi.org/10.1016/j.talanta.2012.11.063

2. Experimental

2.1. Apparatus and reagents

A CHI 660C electrochemical analyzer (Shanghai CH Instrument Company, China), which was in connection with a glassy carbon electrode (GCE), a saturated calomel reference electrode (SCE) and a platinum wire counter electrode, was used for electrochemical measurements. The pH values were measured by a model pHS-25 digital acidometer (Shanghai Leici Factory, China). SEM measurements were carried out on a JSM-6700F scanning electron microscope (Japan Electron Company). X-ray diffraction (XRD) patterns were recorded on a Rigaku (Japan) D/Max r-A X-ray diffractometer with CuKα radiation. Sonifier was adopted for ultrasonic dispersion (KQ 500B, 500 W, Kunshan, China).

Graphite powder (325 mesh, spectral pure, Sinopharm Chemical Reagent Co., China). Thrombin and lysozyme (Shanghai Dingguo Biotechnology Inc., China). LBA (5′-ATC TAC GAA TTC ATC AGG GCT AAA GAG TGC AGA GTT ACT TAG) and thrombin-binding aptamer (TBA, 5′-GGT TGG TGT GGT TGG-3′) were synthesized by Beijing Sunbiotech. Co. Ltd. (China). LBA and TBA were dissolved in Tris-HCl buffer I (25 mmol L^{-1} Tris-HCl, 300 mmol L^{-1} NaCl, pH 6.4). Proteins were prepared in Tris-HCl buffer II (20 mmol L^{-1} Tris-HCl, 140 mmol L^{-1} NaCl, 5 mmol L^{-1} KCl, 5 mmol L^{-1} $MgCl_2$, pH 6.4). Phosphate buffer solution (PBS, 14 mmol L^{-1} NaCl, 0.27 mmol L^{-1} KCl, 1 mmol L^{-1} Na_3PO_4 and 0.176 mmol L^{-1} K_3PO_4). Hexaammineruthenium(III) chloride ($[Ru(NH_3)_6]Cl_3$, Alfa Aesar, China). Solutions were all prepared with Aquapro ultrapure water (resistivity: 18 MΩ cm, Aquaplus AWL-1002-P, Ever Young Enterprises Development Co., Ltd., China) and stored at 4 °C before use.

2.2. Preparation of Fe_2O_3/graphene platform

Graphite oxide (GO) was synthesized from graphite powder by the modified Hummers method as originally presented by Kovtyukhova [22]. In brief, graphite was pre-oxidized by concentrated H_2SO_4, $K_2S_2O_8$, and P_2O_5. Then the pre-oxidized graphite was further re-oxidized by concentrated H_2SO_4 and $KMnO_4$. The as-synthesized GO was suspended in water to obtain a brown dispersion, which was subjected to dialysis for one week to completely remove the residual salts and acids. Graphene oxide (GNO) suspension was obtained by dispersing purified GO in ultrapure water (concentration 0.1 g L^{-1}) with the aid of sonication for 30 min.

GCE (3 mm diameter) was sequentially polished with 0.3 μm and 0.05 μm alumina powder and then washed ultrasonically in water and ethanol for a few minutes, respectively. The cleaned GCE was dried with nitrogen steam for the next modification. GNO/GCE was prepared by casting 15 μL suspension of GNO on GCE surface and dried under an infrared lamp. Graphene/GCE was prepared after GNO/GCE was electrochemically reduced in PBS (pH 7.0) for 600 s at −1.3 V [23]. Electrochemical synthesis of Fe_2O_3 on graphene/GCE was a potentiostatic process (potential of −1.5 V) at 60 °C. Electrolyte was an oxygen-saturated aqueous solution containing 5 mmol L^{-1} $FeCl_3$ and 0.1 mol L^{-1} KCl.

2.3. Fabrication of the sensing interface

Fe_2O_3/graphene/GCE was covered by 10 μL of 10 μmol L^{-1} LBA and kept over night to achieve saturation. Then it was washed with Tris-HCl buffer I and ultrapure water, respectively. The as-prepared electrode was denoted as LBA/Fe_2O_3/graphene/GCE. LBA/Fe_2O_3/graphene/GCE was incubated in a series of thrombin or lysozyme solutions of different concentrations for 1 h.

2.4. Electrochemical measurements

Electrochemical performances of the modified electrodes were evaluated by CV and EIS in $[Fe(CN)_6]^{3-/4-}$. CV was performed at a scan rate of 100 mV s^{-1}. EIS was carried out with AC voltage amplitude of 5 mV, applied potential of 0.172 V, and voltage frequencies ranged from 10 kHz to 1 Hz. Indicator-free EIS was carried out under open-circuit conditions with 0.1 mol L^{-1} PBS used as the supporting electrolyte. All the experiments were conducted at room temperature (25 ± 0.5 °C).

3. Results and discussion

3.1. Electrochemical characterization of Fe_2O_3/graphene/GCE using $[Fe(CN)_6]^{3-/4-}$ redox indicator.

As shown in Fig. 1A, curve a is the CV of $[Fe(CN)_6]^{3-/4-}$ at bare GCE. After bare GCE was coated with GNO, the current responses decrease obviously ascribed to the poor electron transfer ability of GNO (curve b). Due to the electrochemical reduction of GNO, a couple of well-defined redox peaks are observed at graphene/GCE (curve c). Fe_2O_3/graphene/GCE presents the largest redox peaks (curve d). According to Randles-Sevčik equation: $I_{pa}=2.69\times10^5AD^{1/2}n^{3/2}v^{1/2}C$, where I_{pa} refers to the anodic peak current, n the electron-transfer number, A the surface area of the electrode, D the diffusion coefficient, C the concentration of $[Fe(CN)_6]^{3-/4-}$, and v the scan rate [24]. For 1 mmol L^{-1} $[Fe(CN)_6]^{3-/4-}$, $n=1$, $D=6.7\times10^{-6}$ cm^2 s^{-1}, the electroactive areas of GCE, graphene/GCE, and Fe_2O_3/graphene/GCE are determined to be 0.04, 0.11 and 0.15 cm^2, respectively. Obviously, Fe_2O_3/graphene/GCE increases the electroactive surface area as it is approximately 1.36 times larger than that of graphene/GCE. The enhanced surface is benefit to adsorb more LBA and further improve the detection sensitivity. In addition, the redox potential separation of various electrodes shows an increase as follows: Fe_2O_3/grapheme/GCE < graphene/GCE < GCE < GNO/GCE. Usually, the results of EIS can be

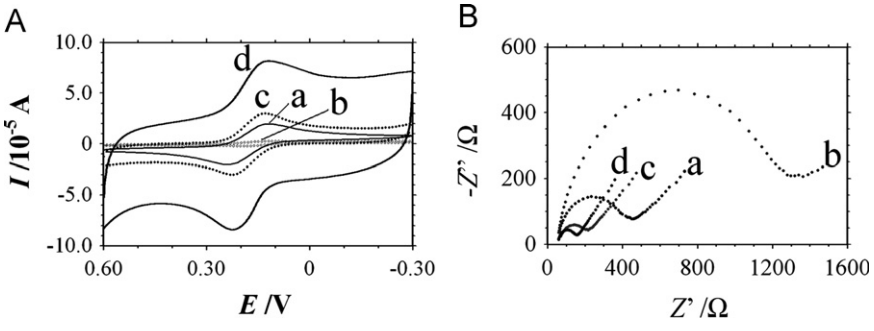

Fig. 1. (A) CVs of 1 mmol L^{-1} $[Fe(CN)_6]^{3-/4-}$ and (B) Nyquist diagrams of 5 mmol L^{-1} $[Fe(CN)_6]^{3-/4-}$ at (a) GCE, (b) GNO/GCE, (c) graphene/GCE and (d) Fe_2O_3/graphene/GCE in 0.1 mol L^{-1} KCl.

illustrated in two different ways: a Nyquist plot or a Bode plot. In Nyquist plot, the semicircle portion at high frequency regions corresponds to the electron transfer limiting process. The electron transfer resistance R_{et} can be measured as the semicircle diameter. In Fig. 1B, when GNO was modified on GCE, the semicircle dramatically increases as compared to bare GCE. After GNO was electrochemically reduced, R_{et} decreases distinctively. Compared with graphene/GCE, R_{et} of Fe_2O_3/graphene/GCE further decreases. The results are consistent with CVs.

3.2. SEM characterization of Fe_2O_3/graphene

The morphologies of Fe_2O_3/graphene were characterized by SEM. Electrochemical deposition of Fe_2O_3 includes the reduction of O_2 at anode and the precipitation of Fe_2O_3 at cathode in an oxygen-saturated solution, i.e., $O_2+2H_2O+4e^-\rightarrow 4OH^-$, $Fe^{3+}+3OH^-\rightarrow Fe(OH)_3$, and $2Fe(OH)_3\rightarrow Fe_2O_3+3H_2O$. In the electrochemical deposition process, graphene (Fig. 2A) with high conductivity had high current flow and large charge density on the electrode surface, leading to high concentration of hydroxide ions, which was beneficial for the growth of Fe_2O_3 [15]. The temperature condition played an obvious role in the formation of Fe_2O_3. Electrochemical deposition of Fe_2O_3 was conducted at different temperatures (20, 30, 40, 50, 60, 70, and 80 °C). The CVs of 1.0 mmol/L $[Fe(CN)_6]^{3-/4-}$ at graphene/GCE before and after electrodeposition were recorded. ΔI_p ($\Delta I_p=I_0-I_{after}$, where I_0 and I_{after} referred to the current obtained before and after the electrochemical deposition of Fe_2O_3, respectively) versus the temperature was plotted (Fig. 3). The largest ΔI_p value was obtained when the electrodeposition was conducted at 60 °C. In morphology, at lower temperature (e.g. 20 °C), the obtained Fe_2O_3 on graphene/GCE does not show regular morphologies (Fig. 2B). When the temperature was changed to 60 °C, the electrochemically deposited Fe_2O_3 exhibits the compact structures with approximate sphere morphologies (Fig. 2C). CV was adopted to investigate the effect of deposition time on the formation of Fe_2O_3 (Fig. 4). With the increase of deposition time, the redox peak currents of $[Fe(CN)_6]^{3-/4-}$ at Fe_2O_3/graphene/GCE increase gradually, and the maximum is obtained at 300 s. The redox peak currents decrease when longer than 300 s. It may be due to the coverage of extremely thick Fe_2O_3 on electrode surface (Fig. 2D), resulting in the depressed conductivity. Thereby, 300 s was selected for the deposition time of Fe_2O_3.

Fig. 5 shows the XRD pattern of Fe_2O_3/graphene. It possesses a weak diffraction at 25.6°, which is assigned to the crystal planes of graphene. The other diffraction peaks at 24.1°, 33.2°, 35.6°, 40.8°, 49.5°, and 54.1° correspond well with the crystal planes of (012), (104), (110), (113), (024), and (116), which can be easily indexed to hexagonal α-Fe_2O_3 (JCPDS 33-664). The XRD results indicate that the crystalline structures of Fe_2O_3 and graphene are maintained in Fe_2O_3/graphene composites.

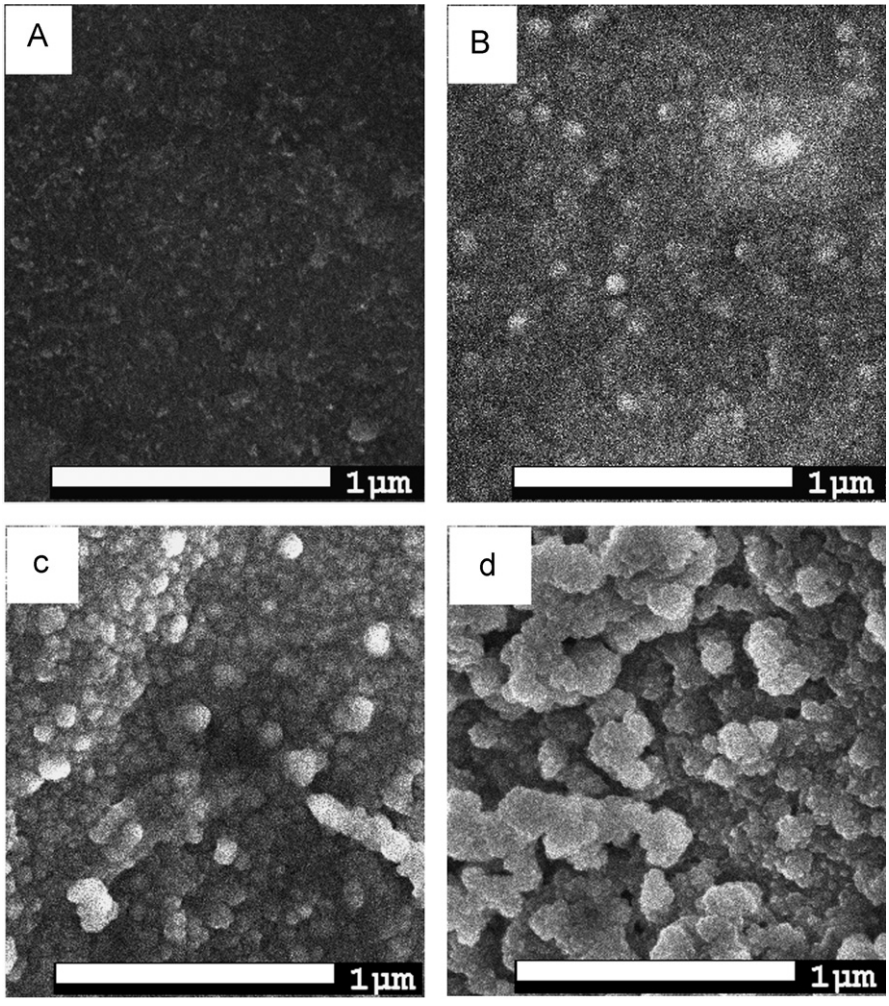

Fig. 2. (A) SEM image of graphene/GCE. SEM images of Fe_2O_3/graphene/GCE prepared by electrodeposition (B) for 300 s at 20 °C, (C) for 300 s at 60 °C, and (D) for 400 s at 60 °C.

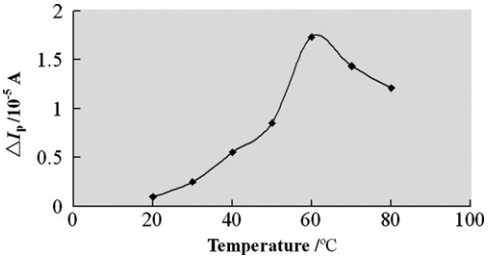

Fig. 3. Effect of the deposition temperature on ΔI_p.

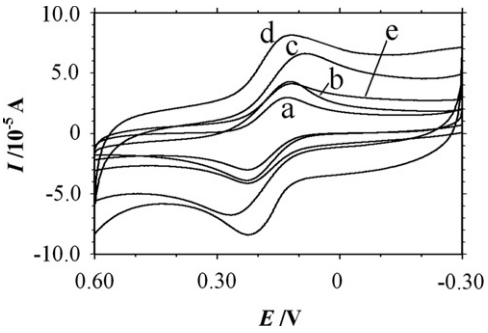

Fig. 4. CVs of 1 mmol L^{-1} $[Fe(CN)_6]^{3-/4-}$ at Fe_2O_3/graphene/GCE prepared by electrodeposition at 60 °C for (a) 0 s, (b) 100 s, (c) 200 s, (d) 300 s, and (e) 400 s, respectively. The supporting electrolyte was 0.1 mol L^{-1} KCl.

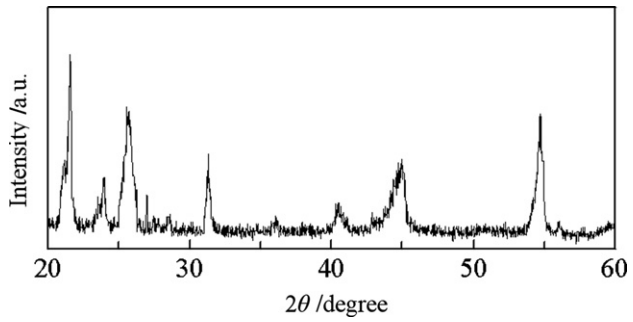

Fig. 5. XRD patterns of Fe_2O_3/graphene composites.

3.3. Indicator-free impedimetric detection of lysozyme

The detection of lysozyme was monitored by EIS in PBS (pH 7.0) without the indicator $[Fe(CN)_6]^{3-/4-}$. In Fig. 6, curve a is the Bode plot of Fe_2O_3/graphene/GCE. The impedance values were measured after the interaction of Fe_2O_3/graphene/GCE with lysozyme (curve b). Compared with Fe_2O_3/graphene/GCE, curve b shows only a very small increment of log$Z$ at high frequency regions, indicating no specific interaction between lysozyme and Fe_2O_3/graphene/GCE. For LBA/Fe_2O_3/graphene/GCE, log$Z$ value is higher than Fe_2O_3/graphene/GCE in high frequency regions (curve c). It indicates that LBA had been successfully immobilized on Fe_2O_3/graphene/GCE. The binding of LBA and lysozyme results in an increase of log$Z$ value in high frequency regions (curve d). It shows that LBA attached on Fe_2O_3/graphene/GCE would catch lysozyme, which induces a barrier for electron transfer. For lysozyme detection, the incubation time of lysozyme was optimized. After LBA/Fe_2O_3/graphene/GCE was immersed into a lysozyme solution for different times, log$Z$ values for every electrode before and after incubation were recorded. The log$Z$ difference (Δlog$Z$) versus incubation time was plotted (Fig. 7). The incubation proceeded with the increase of Δlog$Z$ value. The largest Δlog$Z$ value was obtained when the incubation was conducted for 1 h.

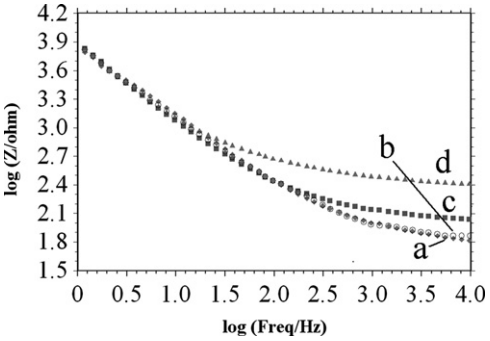

Fig. 6. Bode plots in PBS (pH 7.0) at (a) Fe_2O_3/graphene/GCE, (b) Fe_2O_3/graphene/GCE after the immersion in 5 μg mL^{-1} lysozyme for 1 h, (c) LBA/Fe_2O_3/graphene/GCE, and (d) LBA/Fe_2O_3/graphene/GCE after the immersion in 5 μg mL^{-1} lysozyme for 1 h.

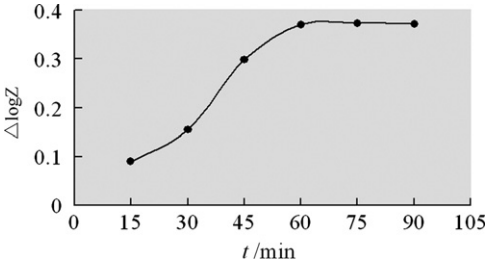

Fig. 7. Influence of the incubation time on Δlog$Z$ signal.

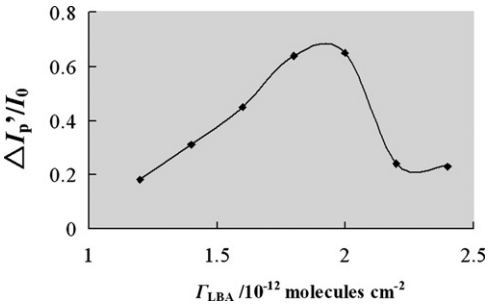

Fig. 8. Sensor signal $\Delta I_p'/I_0$ versus surface density of LBA.

Thus, 1 h was used to make complete interaction between LBA and 5 μg mL^{-1} lysozyme.

$[Ru(NH_3)_6]^{3+}$ was used to study the effect of surface density of LBA on the sensor signal. Thus, a series of LBA/Fe_2O_3/graphene/GCEs with different surface densities were prepared by varying immobilization amount of LBA. The CV measurements of $[Ru(NH_3)_6]^{3+}$ allowed a simple calculation for the surface density of LBA with the charge integrated from the reduction peak from $[Ru(NH_3)_6]^{3+}$ to $[Ru(NH_3)_6]^{2+}$.

The surface concentration of $[Ru(NH_3)_6]^{3+}$, Γ_{Ru}, could be calculated as

$$\Gamma_{Ru} = Q/nFA \quad (1)$$

where Q was the charge obtained by integrating the reduction peak area of surface-bound $[Ru(NH_3)_6]^{3+}$, n was the number of electrons involved in the redox reaction, F was Faraday's constant, and A was the electrode area.

Under saturation conditions, the measured value could be converted to the surface density of LBA, Γ_{LBA}, using the following equation:

$$\Gamma_{LBA} = \Gamma_{Ru}(z/m)N_A \quad (2)$$

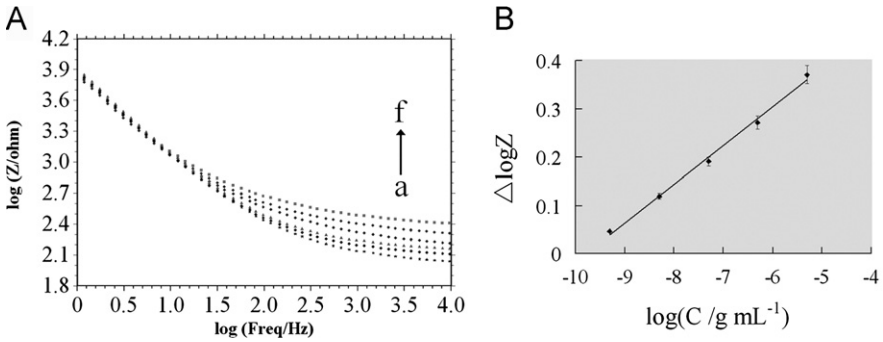

Fig. 9. (A) Bode plots in PBS (pH 7.0) at LBA/Fe_2O_3/graphene/GCE for different concentrations (ng mL^{-1}) of lysozyme: (a) 0, (b) 0.5, (c) 5, (d) 50, (e) 500, and (f) 5000. (B) The plot of $\Delta\log Z$ vs. the logarithm of lysozyme concentrations.

Table 1
Comparison of electrochemical aptasensors for lysozyme.

	This work	Ref. [25]	Ref. [26]
Immobilization platform for LBA	Fe_2O_3/graphene	Gold electrode	Carbon nanotube
Detection method	EIS	EIS	EIS
Detection range	0.5 ng mL^{-1}–5 μg mL^{-1}	0.2 nmol L^{-1}–8 nmol L^{-1}	100 μg mL^{-1}–400 μg mL^{-1}
Detection limit	0.16 ng mL^{-1} (~0.011 nmol L^{-1})	0.07 nmol L^{-1}	12.09 μg mL^{-1}

where z was the valence of the redox cation, m was the number of nucleotides in the LBA, and N_A was Avogadro's constant. This equation had the same assumptions and conditions as Eq. (1).

Fig. 8 shows the correlation between the sensor signal $\Delta I_p'/I_0$ ($\Delta I_p'=I_0 - I_{after}$, where I_0 and I_{after} referred to the current obtained before and after LBA/Fe_2O_3/graphene/GCE incubated with lysozyme, respectively) and the surface density of LBA. From the plot, it is indicative that the sensor sensitivity is clearly dependent on the LBA surface density: as the surface density increases, $\Delta I_p'/I_0$ ratio increases to a maximum and then decreases substantially. At higher surface density, the binding of lysozyme to LBA is hindered due to spatial restriction for the DNA strand to fold into the aptamer configuration to bind to the fairly large lysozyme protein. For lower surface density, this is no longer a concern. Therefore, the ideal surface density for this aptasensor is between 1.8×10^{-12} and 2.0×10^{-12} molecules cm^{-2}.

In Fig. 9, the impedance signals increase with the increase of lysozyme concentration. The log$Z$ difference ($\Delta\log Z$) between LBA/Fe_2O_3/graphene/GCE and LBA/Fe_2O_3/graphene/GCE incubated with lysozyme is adopted to evaluate the responses to lysozyme. There is a linear relationship between $\Delta\log Z$ and logarithm of lysozyme concentration (C) from 0.5 ng mL^{-1} to 5 μg mL^{-1}. The regression equation is $\Delta\log Z=0.0802\log C+0.7851$ ($R=0.995$). The detection limit is evaluated as 0.16 ng mL^{-1} corresponding to signal/noise ratio of 3. It is important to note that, at higher concentrations of lysozyme (e.g., 5–20 μg mL^{-1}), the quantification of impedance signals is not reproducible (data not shown). It indicates that the response mechanism may become more complex (involving nonspecific interactions between the protein and the aptamer). The aptasensor in this work is compared with other electrochemical aptasensors reported in literatures (Table 1). This aptasensor shows a lower detection limit and wider dynamic detection range than others.

Control experiments were performed to reveal the selectivity and specificity of the aptasensor. LBA/Fe_2O_3/graphene/GCE was immersed in 0.5 μg mL^{-1} thrombin, 0 g mL^{-1} lysozyme, and 0.5 μg mL^{-1} lysozyme under the same experimental conditions, respectively. Different impedance signals were obtained in Fig. 10. After the incubation of thrombin with LBA/Fe_2O_3/graphene/GCE (column b), the log$Z$ value is calculated as 2.051, a small higher than LBA/Fe_2O_3/graphene/GCE (column a). The log$Z$ value (column c) is calculated as 2.055 after immersion in Tris-HCl buffer II. The interaction between lysozyme and LBA/Fe_2O_3/graphene/GCE leads to a 17.2% increase of the log$Z$ value (column d). The "signal on" results are similar to the report published elsewhere [27]. It indicates that the aptasensor has a high selectivity.

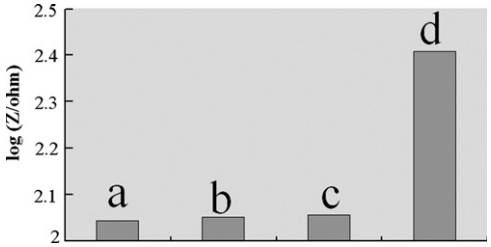

Fig. 10. Control experiments for (a) LBA/Fe_2O_3/graphene/GCE after the immersion in (b) 0.5 μg mL^{-1} thrombin, (c) Tris-HCl buffer II, and (d) 0.5 μg mL^{-1} lysozyme, respectively.

Another control experiment was performed to ensure that lysozyme did not bind to other sequences of DNA. TBA was immobilized on Fe_2O_3/graphene/GCE, and the impedance was recorded. After TBA/Fe_2O_3/graphene/GCE exposure to 0.5 μg mL^{-1} lysozyme for 1 h, a 2.25% increase in log$Z$ is shown after exposure to lysozyme, implying that TBA/Fe_2O_3/graphene/GCE did not produce a complex with lysozyme, and lead to significant changes in the impedance spectrum.

3.4. Stability and repeatability of the aptasensor

The stability of LBA/Fe_2O_3/graphene/GCE is a crucial factor to achieve high sensitivity. The LBA/ Fe_2O_3/graphene/GCE was incubated in PBS (pH 7.0), Tris-HCl buffer I, and Tris-HCl buffer II at 25 °C for 10 h, respectively. Then the impedance was recorded in PBS (pH 7.0), and the obtained signals almost remain unchanged compared with the unincubated electrode. The LBA/Fe_2O_3/graphene/GCE was stored at 4 °C for 10 days, and the decrease of the impedance signal is got as 4.48%. In addition, ten repetitive impedance measurements of LBA/Fe_2O_3/graphene/GCE were

performed in PBS (pH 7.0). A relative standard deviation (RSD) of 2.86% for log$Z$ value is obtained. The results demonstrate that the prepared aptasensor has good stability.

The repeatability of aptasensor is highly significant in protein assay. Six parallel-fabricated LBA/Fe_2O_3/graphene/GCEs were performed to detect 0.5 μg mL^{-1} lysozyme. Bode plots of these electrodes before and after detection were recorded. A RSD of 4.23% for Δlog$Z$ value is evaluated.

4. Conclusion

In conclusion, a sensitive indicator-free electrochemical aptasensor based on Fe_2O_3/graphene matrix was developed for the first time. The as-prepared aptasensor has several advantages: (1) Fe_2O_3/graphene with three-dimensional structure brings in more molecular recognition elements (as a model here, LBA), which can improve the sensitivity of aptasensor; (2) indicator-free impedance technique exhibits a very simple and promising detection method; (3) such an aptamer immobilization platform is demonstrated as a new way in electrochemical aptasensors.

Acknowledgments

This project was supported by the National Natural Science Foundation of China (Nos. 20805025, 20975057 and. 21275084), Doctoral Foundation of the Ministry of Education of China (No. 20113719130001), Outstanding Adult-Young Scientific Research Encouraging Foundation of Shandong Province (No. BS2012CL013), and Scientific and Technical Development Project of Qingdao (No. 12-1-4-3-(23)-jch).

References

[1] K.S. Novoselov, A.K. Geim, S.V. Morozov, D. Jiang, Y. Zhang, S.V. Dubonos, I.V. Grigorieva, A.A. Firsov, Science 306 (2004) 666–669.
[2] X. Huang, Z.Y. Yin, S.X. Wu, X.Y. Qi, Q.Y. He, Q.C. Zhang, Q.Y. Yan, F. Boey, H. Zhang, Small 7 (2011) 1876–1902.
[3] V. Singh, D. Joung, L. Zhai, S. Das, S.I. Khondaker, S. Seal, Progress in Materials Science 56 (2011) 1178–1271.
[4] D. Du, J. Liu, X.Y. Zhang, X.L. Cui, Y.H. Lin, Journal of Materials Chemistry 21 (2011) 8032–8037.
[5] S.M. Paek, E.J. Yoo, I. Honma, Nano letters 9 (2009) 72–75.
[6] D.H. Wang, D. Choi, J. Li, Z.G. Yang, Z.M. Nie, R. Kou, D.H. Hu, C.M. Wang, L.V. Saraf, J.G. Zhang, I.A. Aksay, J. Liu, ACS Nano 3 (2009) 907–914.
[7] Y.P. Zhang, H.B. Li, L.K. Pan, T. Lu, Z. Sun, Journal of Electroanalytical Chemistry 634 (2009) 68–71.
[8] S. Yang, X. Feng, S. Ivanovici, K. Müllen, Angewandte Chemie-International Edition 49 (2010) 8408–8411.
[9] Z.S. Wu, D.W. Wang, W.C. Ren, J.P. Zhao, G.M. Zhou, F. Li, H.M. Cheng, Advanced Functional Materials 20 (2010) 3595–3602.
[10] M.A. Rafiee, J. Rafiee, I. Srivastava, Z. Wang, H.H. Song, Z.Z. Yu, N. Koratkar, Small 6 (2010) 179–183.
[11] A.S. Adekunle, B.O. Agboola, J. Pillay, K.I. Ozoemena, Sensors and Actuators B-Chemical 148 (2010) 93–102.
[12] S.W. Cao, Y.J. Zhu, Journal of Physical Chemistry C 112 (2008) 6253–6257.
[13] Z. Zhou, Y. Xu, M. Hojamberdiev, W. Liu, J. Wang, Journal of Alloys and Compounds 507 (2010) 309–311.
[14] L.C. Yang, W.L. Guo, Y. Shi, Y.P. Wu, Journal of Alloys and Compounds 501 (2010) 218–220.
[15] R.K. Joshi, J.J. Schneider, Chemical Society Reviews 41 (2012) 5285–5312.
[16] Z.Y. Yin, S.X. Wu, X.Z. Zhou, X. Huang, Q.C. Zhang, F. Boey, H. Zhang, Small 6 (2010) 307–312.
[17] S.X. Wu, Z.Y. Yin, Q.Y. He, X. Huang, X.Z. Zhou, H. Zhang, Journal of Physical Chemistry C 114 (2010) 11816–11821.
[18] B. Lindholm-Sethson, J. Nyström, M. Malmsten, L. Ringstad, A. Nelson, P. Geladi, Analytical and Bioanalytical Chemistry 398 (2010) 2341–2349.
[19] N.S. Mathebula, J. Pillay, G. Toschi, J.A. Verschoor, K.I. Ozoemena, Chemical Communications (2009) 3345–3347.
[20] T.L. Lasseter, W. Cai, R.J. Hamers, Analyst 129 (2004) 3–8.
[21] C.P. Chen, A. Ganguly, C.H. Wang, C.W. Hsu, S. Chatto-padhyay, Y.K. Hsu, Y.C. Chang, K.H. Chen, L.C. Chen, Analytical Chemistry 81 (2009) 36–42.
[22] N.I. Kovtyukhova, P.J. Ollivier, B.R. Martin, T.E. Mallouk, S.A. Chizhik, E.V. Buzaneva, A.D. Gorchinskiy, Chemistry of Materials 11 (1999) 771–778.
[23] M. Du, T. Yang, K. Jiao, Journal of Materials Chemistry 20 (2010) 9253–9260.
[24] F. Xiao, F.Q. Zhao, J.W. Li, L.Q. Liu, B.Z. Zeng, Electrochimica Acta 53 (2008) 7781–7788.
[25] Y.G. Peng, D.D. Zhang, Y. Li, H.L. Qi, Q. Gao, C.X. Zhang, Biosensors and Bioelectronics 25 (2009) 94–99.
[26] F. Rohrbach, H. Karadeniz, A. Erdem, M. Famulok, G. Mayer, Analytical Biochemistry 421 (2012) 454–459.
[27] Z.B. Chen, L.D. Li, H.T. Zhao, L. Guo, X.J. Mu, Talanta 83 (2011) 1501–1506.